Accurate Azimuth Ground Deformation Estimation from Sentinel-1 Time Series

Nestor Yague-Martinez, Pau Prats-Iraola, *Senior Member, IEEE*

***Abstract*—This letter proposes the exploitation of the overlapping areas between bursts of Sentinel-1 Interferometric Wide swath data for the estimation of ground azimuth deformation velocities from time series, which provides high sensitivity to the North-South direction. The availability of two separated Doppler spectral looks over these areas allows one to obtain high accurate estimates, overcoming the limited performance of classical correlation techniques with coarse resolution modes. Since the estimation is restricted to the (sparsely distributed) burst overlaps, its applicability is limited to geophysical phenomena characterized by a slow spatial variability, e.g., seismic scenarios. We demonstrate the suitability of this approach to time series over a region in Pakistan affected by post-seismic deformation. The estimated mean azimuth velocity performance from real data indicates an accuracy better than 7 mm/year over high long-term coherent areas for a three-year data stack.**

***Index Terms*—Synthetic aperture radar, TOPS, Sentinel-1, interferometry, overlaps, ESD, time series, azimuth ground deformation, Balochistan.**

I. Introduction

THE application of correlation techniques to spaceborne synthetic aperture radar (SAR) image pairs to obtain sensitivity to ground deformation in the azimuth direction, traditionally used with spaceborne StripMap images [1], provides a poor accuracy with the Sentinel-1 Interferometric Wide swath (IW) mode. The poor performance results from the low azimuth resolution of Sentinel-1 IW, namely, 20 m [2], restricting its use to co-seismic events, e.g., strong earthquakes, where the displacements are expected to be in the order of a few meters. Sentinel-1 IW products employ the Terrain Observation by Progressive Scans (TOPS) acquisition baseline [3].

An alternative to cross-correlation techniques consists in the exploitation of spectral diversity (SD) techniques [4] applied to the overlap regions between bursts of TOPS data [5][6], where two separated slices of the Doppler spectrum are available. The burst overlaps have been traditionally exploited to refine the azimuth coregistration parameters due to orbital inaccuracies with pairs [5] and also extended to stacks of data [7][8] in order to mitigate temporal decorrelation effects.

Regarding the estimation of ground deformation, the burst overlaps have been also exploited with interferometric pairs of Sentinel-1 IW for the retrieval of azimuth displacements from strong earthquakes or for post-seismic deformation estimation with a very large temporal baseline [9][10][11].

The opportunity to retrieve continuous accurate azimuth shifts exploiting Doppler spectrum diversity following the TOPS acquisition baseline has been already proposed with the 2-look TOPS modes (TOPS2 and TOPS2+) and demonstrated with TerraSAR-X [12]. The trade-off of these approaches is a reduced coverage in elevation or/and azimuth resolution.

Our contribution in this letter focuses on the retrieval of azimuthal ground displacements with Sentinel-1 IW data over slow deforming tectonic scenarios exploiting the burst overlaps, making use of stacks of images. The sparse coverage of the measurements on the burst overlaps implies a discontinuous azimuth deformation retrieval, but very valuable for scenarios with smooth gradients of spatial deformation. We perform a 2-D interpolation of the mean azimuth velocity over the gaps between overlaps, to allow a better visual interpretation, however in a real scenario an inversion with a geophysical model is usually performed, employing the original measurements. Compared to the work done in [9][10][11], which applies a full persistent scatterer interferometry (PSI) processing to the overlap areas, our approach takes advantage of the fact that the double differential phases exploiting the overlap areas are autocalibrated and most of the tropospheric contributions cancel out.

The paper is structured as follows: in section II the methodology is presented. Section III provides the expected performances with the Sentinel-1 system. In Section IV post-seismic deformation results with three years of Sentinel-1 IW time-series data over Balochistan, Pakistan, are presented.

II. Methodology

SAR images acquired with the TOPS mode take place by recording subsets of echoes of the full aperture, called *bursts* [3]. Our starting point consists in a stack of N single look complex (SLC) images with M bursts per subswath, from Sentinel-1 IW images, whose bursts have been geometrically coregistered using precise orbital information and an external digital elevation model (DEM) [13].

A. Estimation of azimuth shifts

The spectral separation for a target on ground located at the overlapping area between two consecutive bursts can be exploited to retrieve an accurate estimation of the azimuthal shift. The azimuth shifts can be estimated by computing the enhanced spectral diversity (ESD) [5][6] phases. This can be

Manuscript received October 22, 2021; revised December 23, 2021 and February 15, 2022; accepted March 16, 2022

This work was supported partially by ESA under Contract 4000110587/14/I-BG.

N. Yague-Martinez was with the German Aerospace Center (DLR), Oberpfaffenhofen D-82234, Germany. He is now with Capella Space Corp. (e-mail: nestor.yague@gmail.com)

Pau Prats-Iraola is with the German Aerospace Center (DLR), Oberpfaffenhofen D-82234, Germany. (e-mail: pau.prats@dlr.de)

done for each pixel with range and azimuth coordinates r and x, respectively, at the overlapping areas from consecutive bursts according to

$$\begin{aligned}\phi^k_{\mathrm{ESD}}(r,x) = \arg\Big\{ &\left[p_i(r,x)\cdot(s^k_i(r,x))^*\right]\cdot \\ &\left[p_{i+1}(r,x)\cdot(s^k_{i+1}(r,x))^*\right]^*\Big\} \\ (r,x) &\in (p_i \cap s_i)\cap(p_{i+1}\cap s_{i+1}) \\ k &= 0..N-2 \\ i &= 0..M-2,\end{aligned} \tag{1}$$

where p_{i} and s_{i} refer to the i^{th} burst of the primary and secondary images, respectively, and $p_{\mathrm{i+1}}$ and $s_{\mathrm{i+1}}$ to the $(i+1)^{\mathrm{th}}$ burst in an analogous way. The superscript k indicates the index of the secondary images and $\arg\{\cdot\}$ retrieves the phase of a complex number. N indicates the number of images in the stack and M the number of burst overlaps. Given a desired output product resolution, spatial multilooking can be applied to the computation of the interferometric and ESD phases.

B. Mean azimuth velocity estimation

In [12] two approaches were proposed for the retrieval of the mean azimuth velocity when exploiting 2-look systems, namely: (i) to obtain the mean line-of-sight velocities for each look independently (PSI processing) and perform the difference and scale the result, or (ii) to work directly with the ESD phases. We develop in the following the latter approach, which has the major advantage that the ESD phases are already autocalibrated. This means that systematic effects, such as the constant phase offset, residual topography errors and tropospheric noise cancel out. Since the phases are already autocalibrated there is no need to establish a reference point to align the ESD interferograms or to exploit arcs between points, to accommodate temporal variations of the troposphere, susceptible to introduce wrapping errors for very sparse networks.

The azimuth shift (in spatial units) for the k interferogram, $\Delta x^k(r,x)$, can be obtained based on the relation [5]

$$\phi^k_{\mathrm{ESD}}(r,x) = 2\pi\Delta f_{\mathrm{ovl}}\frac{\Delta x^k(r,x)}{v_{\mathrm{g}}} \tag{2}$$

where Δf_{ovl} is the Doppler spectral separation between consecutive bursts at its overlapping area, and v_{g} is the radar beam ground velocity of the reference acquisition. Note that both magnitudes present a dependence with range, r, omitted for the sake of simplicity.

The estimation of the mean azimuth velocity, v_a, can be obtained for each multilooked pixel by applying the periodogram to the ESD phases of the time-series as follows

$$\widehat{v_{\mathrm{a}}} = \arg\max_{v_{\mathrm{a}}}\left\{\Re\left\{\sum_{k=0}^{N-2} e^{j(\phi_{\mathrm{ESD}}[k]-2\pi\Delta f_{\mathrm{ovl}}v_{\mathrm{a}}T[k]v_{\mathrm{g}})}\right\}\right\}, \tag{3}$$

where $\arg\max_{v_{\mathrm{a}}}\{\cdot\}$ stands for the argument of the maximum (mean azimuth velocity, v_{a}, for which the function attains its largest value). ϕ_{ESD} is the temporal array of ESD phases of each (primary-secondary) interferogram, and T is an array containing the temporal baselines of each interferogram. Eq. (3) is computed for each multilooked pixel, and again, the dependence of v_{a}, ϕ_{ESD}, Δf_{ovl} and v_{g} with range and azimuth has been omitted for simplicity. Note that any other deformation model other than linear might be used instead of assuming linear deformation. Uncompensated azimuthal orbital errors have a small impact on the estimation of the mean azimuth velocity if the number of images is large enough and the magnitude of the deformation signal large enough.

C. Azimuthal residual errors

Once the mean azimuth velocity has been obtained, the residual azimuth error (in spatial units) for each interferogram, k, can be easily retrieved, by combining (2) and (3), as

$$\Delta x_{\mathrm{res}}[k] = \frac{v_{\mathrm{g}}[k]}{2\pi\Delta f_{\mathrm{ovl}}}\phi_{\mathrm{ESD}}[k] - v_{\mathrm{a}}T[k] \tag{4}$$

The retrieved azimuth errors include azimuth orbital errors, azimuth shifts introduced by the differential ionosphere and any non-linear deformation component. The differential ionospheric artifacts can be mitigated beforehand exploiting the (range) split-spectrum method [14] to the coregistered SLCs. Since orbital along-track errors are almost constant within a scene, an average of all estimates for a particular interferogram k would result in the differential orbital error for that particular epoch. After removing these contributions, the ESD phases contain essentially the complete deformation time series, since the tropospheric component, which is the main limitation in conventional PSI, is almost absent. Considering scenarios with low deformation rates and based on the sensitivity of the ESD phases (wrapping occurs for displacements larger than ± 70 cm [6]) the temporal unwrapping of the time series for each pixel of interest does not pose a critical step.

III. Expected Performance

This section provides the achievable accuracy in the retrieval of azimuth shifts, applying the methodology previously exposed, and makes a comparison to the accuracy achievable using conventional cross-correlation methods. We assume in the following homogeneous interferometric SAR images, which are characterized by distributed scatterers with Gaussian statistics and partial coherence.

A. Interferometric pairs

The achievable accuracy to retrieve the azimuth shifts (in spatial units) from interferometric pairs exploiting ESD at the overlapping regions between consecutive bursts is given by [15][5]

$$\begin{aligned}\sigma_{\Delta x} &= \frac{\sigma_{\phi_{\mathrm{ESD}}}}{2\pi\Delta f_{\mathrm{ovl}}(r)}v_{\mathrm{g}}(r) \\ &= \frac{1}{2\pi\Delta f_{\mathrm{ovl}}\sqrt{L}}\frac{\sqrt{1-\gamma^2}}{\gamma}v_{\mathrm{g}}(r),\end{aligned} \tag{5}$$

where $\sigma_{\phi_{\mathrm{ESD}}}$ is the standard deviation of the ESD phase, L is the number of averaged samples (spatial looks) and γ the interferometric coherence. We assume that the number of looks is large enough, i.e. $L \to \infty$, such that the asymptotic approximation of the phase standard deviation is fulfilled.

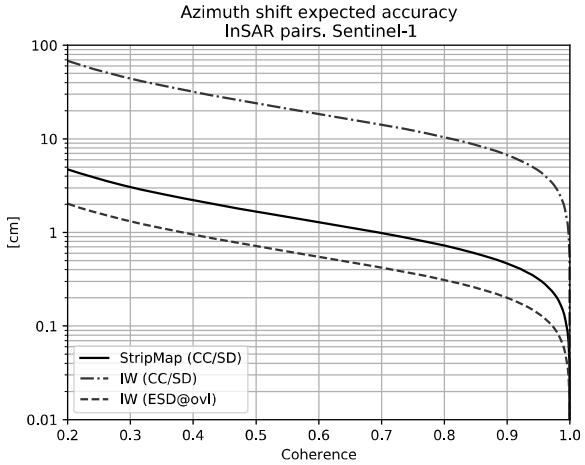

Fig. 1: Expected accuracy for the estimation of the azimuth shift with the Sentinel-1 system, from interferometric pairs, with ESD with IW and employing cross correlation (CC) with StripMap and IW. The product resolution is 500 m $\times$ 500 m.

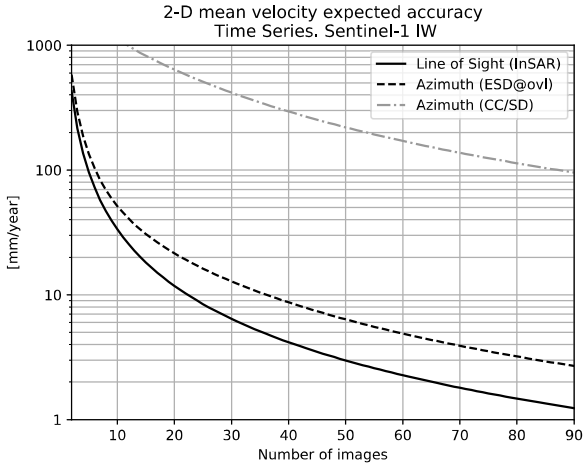

Fig. 2: Expected mean ground velocity displacement performance in the line-of-sight and azimuth directions by exploiting ESD at the burst overlapping areas with Sentinel-1 IW time series, assuming a repetition cycle of 12 days. An exponential decorrelation model has been used with a time constant of 40 days, a long-term coherence equal to 0.2 and a standard deviation of the turbulent troposphere equal to 1 cm. The product resolution has been set to 500 m $\times$ 500 m. The achievable accuracy using SD is also displayed for comparisons purposes.

TABLE I: Relevant Sentinel-1 system parameters for the retrieval of azimuth shifts. The Doppler bandwidth of each look, $B_{\rm look}$, and spectral separation, Δf, for the IW2 subswath and for StripMap are provided. A product resolution of 500 m $\times$ 500 m has been established, being L the number of spatial looks. $\sigma/\sigma_{\rm SM}$ indicates the ratio of accuracies with respect to StripMap (SM). The last row provides the ambiguity bands for phase-based methods (SD or ESD); this does not apply to CC, which provides an absolute measurement.

Sentinel-1 system	StripMap	IW	
Resolution (rg$\times$az) [m]	1.7$\times$4.3	2.7$\times$23	
Measurement techn.	CC/SD	CC/SD	ESD
Azimuth Coverage	full	full	overlaps
$B_{\rm look}$[Hz]	526.7	104.3	313
Δf[Hz]	1053.3	208.7	4045
L (500 m$\times$500 m)	11364	1394	4183
$\sigma/\sigma_{\rm SM}$	1	11.34	0.34
Amb. band [m]	$-/\pm$3.2	$-/\pm$16.3	$\pm$0.8

The curves of Fig. 1 show the achievable azimuth shift retrieval accuracy for pairs of Sentinel-1 images. The accuracy that can be obtained with the StripMap mode using cross-correlation (CC) [1] techniques is also displayed for reference.

Table I summarizes the spectral separation and available bandwidth for the Sentinel-1 system. The application of conventional cross-correlation (or equivalently taking sublooks from the original spectrum [4]) to IW data provides an accuracy one order of magnitude worse than for StripMap, whereas exploiting the overlaps reduces the standard deviation ratio to $1/3$ when compared to StripMap. The standard deviation ratio between ESD at the burst overlaps and cross-correlation with IW is reduced to 0.03 (an improvement by a factor 33, i.e. 30.4 dB).

[1]Note that the accuracies of CC and SD, with the optimum bandwidth ratio $b = B/3$, are identical, as demonstrated in [15]; b stands for the sub-look bandwidth, whereas B is the available bandwidth

B. Time series

The exploitation of time series enables the retrieval of very small ground displacements by means of the estimation of the mean deformation velocity. The expected 2-D (line of sight and azimuth) accuracies, including the influence of the turbulent troposphere, are provided in the following. The turbulent troposphere can be modeled as a noise source of certain power in the radar line of sight.

When the burst overlaps of Sentinel-1 IW data are exploited to obtain azimuth displacements, two repeat-pass interferograms are available, containing each of them almost the same tropospheric delay because of the small temporal (2.3 s) and spatial (20 m at 1 km height) baselines between observations of the same overpass. In [16] a quantitative analysis for the case of simultaneous squinted SAR acquisitions with two platforms has been provided, being straightforward its extension to our burst-overlaps case.

Fig. 2 shows the performance curves of the mean velocities for the azimuth and line of sight directions as a function of the number of images in the stack.

The achievable accuracies in the line of sight and azimuth are closer for short stacks. The reason is that the azimuth estimation is much less affected by turbulent troposphere, due to the high spatial and temporal correlation between observations, whereas the estimation in the line-of-sight direction is strongly affected by the troposphere, as it cannot be mitigated properly due to the reduced number of images. Adding more images to the stack enhances the estimation in line of sight, whereas the azimuth direction improves only due to having more realizations (images).

IV. Results with Sentinel-1 data

We present in this section results with stacks of images in ascending and descending geometry over Balochistan, in Pakistan. This area was affected by strong Earthquakes in November 2013 [17], followed by post-seismic displacement in the North-South direction, as has been retrieved from experimental TerraSAR-X 2-look TOPS time series [12].

Sentinel-1 IW images were available over the area starting at the end of 2014. Two data take slices have been processed for each geometry, resulting in a coverage of 250 km $\times$ 340 km.

The ascending dataset consists of 50 acquisitions and covers a time span of approximately three years, from 25 October 2014 until 27 September 2017. The primary image has been selected on 23 May 2016. Fig. 3(a) shows a Google Earth representation with a gray-scale optical basemap in the background including the colour-coded deformation estimates at the overlap regions. The smooth spatial variation of the displacement allows performing an interpolation with a 2-D linear kernel between overlaps, for better visual interpretation, shown in Fig. 3(c).

The descending dataset consists also of 50 acquisitions and covers a similar time span, from 16 October 2014 until 13 August 2017. The primary image dates 27 March 2016. Figures 3(b) and (d) show the descending results analogously to the ascending results. For both geometries the 2013 surface rupture line is depicted with a black solid line, indicating that the deformation pattern of the post-seismic deformation is in concordance with the 2013 co-seismic deformation.

At the bottom of the figure, a performance assessment is provided for both geometries. For each multilooked pixel, an exponential decorrelation model [18] has been applied in order to retrieve the long-term coherence, which has been used to compute the standard deviation for different bins. This is done for each subswath (IW1-3) and for the whole scene (ALL). The Cramér Rao Bound (CRB) [16] is displayed for reference. The deviations between measurements and expected performance might be due to not having performed a joint estimation of the ESD phases with the Phase Linking [19] algorithm and assumptions on the troposphere, namely, its autocorrelation function, height and wind speed. The deviations are larger for low long-term coherence values probably due to biased coherence estimation employing a limited number of samples. For high long-term coherences (> 0.5) the accuracy is better than approximately 7 mm/year for both geometries.

V. Conclusions

The exploitation of the burst overlaps of Sentinel-1 IW acquisitions represents an opportunity to obtain accurate estimates of along-track ground displacements. The coverage of the estimation is restricted to the overlap regions making it suitable for the study of large scale deformation phenomena, e.g., strain, co-seismic events, etc. The proposed approach exploits the particular characteristics of the ESD phases, namely, the fact that these phases are autocalibrated and that most of the tropospheric signal cancels out. This allows a significant simplification of the processing to retrieve the deformation time series when compared to conventional PSI approaches.

The along-track estimation complements the line-of-sight deformation measurement and aids to the computation of a more homogeneous 3D deformation retrieval, which can be of valuable interest for geophysical applications [10][11].

This procedure has been applied to two three-years stacks of Sentinel-1 images over Balochistan, revealing an accuracy better than 7 mm/year for high coherent areas, which can even be improved using a joint estimation of the ESD phases.

References

[1] R. Michel *et al.*, "Measuring ground displacements from SAR amplitude images: Application to the Landers earthquake," *Geophys. Res. Lett., 26(7), 875–878.*, 1999.

[2] R. Torres *et al.*, "The Sentinel-1 mission and its application capabilities," in *Geoscience and Remote Sensing Symposium (IGARSS), 2012 IEEE International*, July 2012, pp. 1703–1706.

[3] F. De Zan and A. Monti Guarnieri, "TOPSAR: Terrain Observation by Progressive Scans," *Geoscience and Remote Sensing, IEEE Transactions on*, vol. 44, no. 9, pp. 2352–2360, Sept 2006.

[4] R. Scheiber and A. Moreira, "Coregistration of interferometric SAR images using spectral diversity," *Geoscience and Remote Sensing, IEEE Transactions on*, vol. 38, no. 5, pp. 2179–2191, Sep 2000.

[5] P. Prats-Iraola *et al.*, "TOPS Interferometry with TerraSAR-X," *Geoscience and Remote Sensing, IEEE Transactions on*, vol. 50, no. 8, pp. 3179–3188, Aug 2012.

[6] N. Yague-Martinez *et al.*, "Interferometric Processing of Sentinel-1 TOPS Data," *IEEE Transactions on Geoscience and Remote Sensing*, vol. 54, no. 4, pp. 2220–2234, April 2016.

[7] N. Yague-Martinez *et al.*, "Coregistration of Interferometric Stacks of Sentinel-1 TOPS Data," *IEEE Geoscience and Remote Sensing Letters*, vol. 14, no. 7, pp. 1002–1006, July 2017.

[8] H. Fattahi *et al.*, "A Network-Based Enhanced Spectral Diversity Approach for TOPS Time-Series Analysis," *IEEE Transactions on Geoscience and Remote Sensing*, vol. 55, no. 2, pp. 777–786, Feb 2017.

[9] A. Hooper and K. Spaans, "Sentinel-1 along-track InSAR for global strain rate estimation," in *FRINGE 2017*, http://fringe2017.esa.int/files/presentation523.pdf.

[10] A. Hooper *et al.*, "The improvement to high-resolution maps of interseismic strain accumulation from incorporating Sentinel-1 along-track measurements," in *AGU Fall Meeting Abstracts*, vol. 2020, 2020, pp. G018–07.

[11] A. Hooper *et al.*, "Large-scale, high-resolution maps of interseismic strain accumulation from Sentinel-1, and incorporation of along-track measurements," in *EGU General Assembly Conference Abstracts*, 2021, pp. EGU21–15 946.

[12] N. Yague-Martinez *et al.*, "The 2-Look TOPS Mode: Design and Demonstration With TerraSAR-X," *IEEE Transactions on Geoscience and Remote Sensing*, vol. 57, no. 10, pp. 7682–7703, 10 2019.

[13] E. Sansosti *et al.*, "Geometrical SAR image registration," *Geoscience and Remote Sensing, IEEE Transactions on*, vol. 44, no. 10, pp. 2861–2870, Oct 2006.

[14] G. Gomba *et al.*, "Ionospheric Phase Screen Compensation for the Sentinel-1 TOPS and ALOS-2 ScanSAR Modes," *IEEE Transactions on Geoscience and Remote Sensing*, vol. 55, no. 1, pp. 223–235, Jan 2017.

[15] R. Bamler and M. Eineder, "Accuracy of differential shift estimation by correlation and split-bandwidth interferometry for wideband and delta-k SAR systems," *Geoscience and Remote Sensing Letters, IEEE*, vol. 2, no. 2, pp. 151–155, April 2005.

[16] P. Prats-Iraola *et al.*, "Performance of 3-D Surface Deformation Estimation for Simultaneous Squinted SAR Acquisitions," *IEEE Transactions on Geoscience and Remote Sensing*, vol. PP, no. 99, pp. 1–12, 2017.

[17] J.-P. Avouac *et al.*, "The 2013, Mw 7.7 Balochistan earthquake, energetic strike-slip reactivation of a thrust fault," *Earth and Planetary Science Letters*, 2014.

[18] F. Rocca, "Modeling Interferogram Stacks," *Geoscience and Remote Sensing, IEEE Transactions on*, vol. 45, no. 10, pp. 3289–3299, Oct 2007.

[19] A. M. Guarnieri and S. Tebaldini, "On the Exploitation of Target Statistics for SAR Interferometry Applications," *IEEE Transactions on Geoscience and Remote Sensing*, vol. 46, no. 11, pp. 3436–3443, Nov 2008.

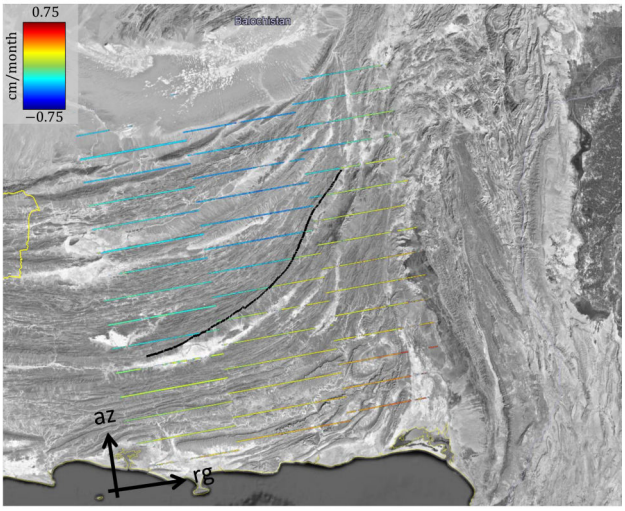

(a) Ascending. Mean azimuth velocity at overlaps

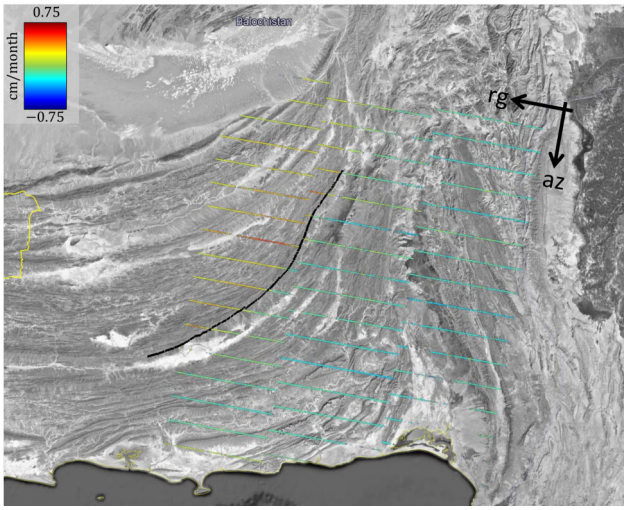

(b) Descending. Mean azimuth velocity at overlaps

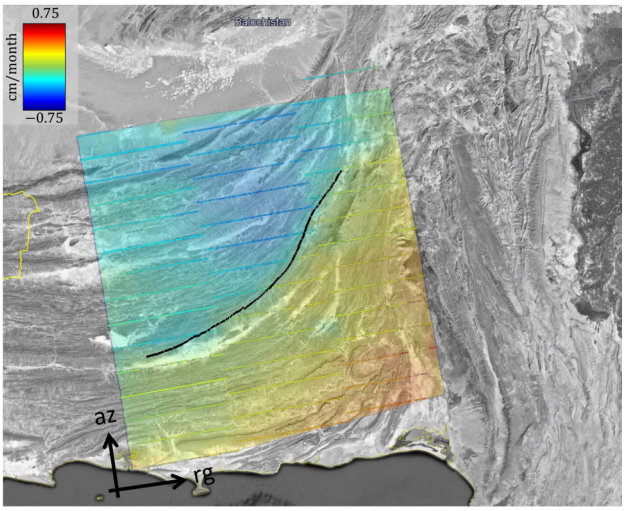

(c) Ascending. Interpolated mean azimuth velocity

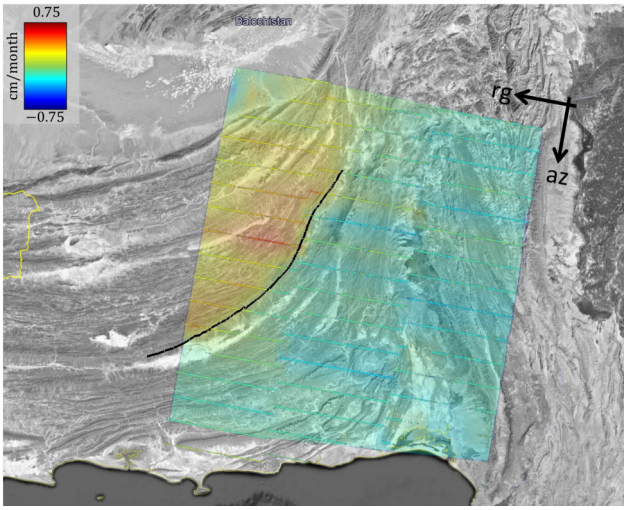

(d) Descending. Interpolated mean azimuth velocity

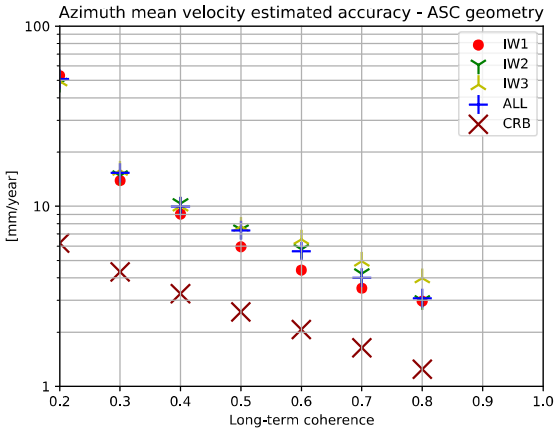

(e) Ascending. Standard deviation of mean azimuth velocity

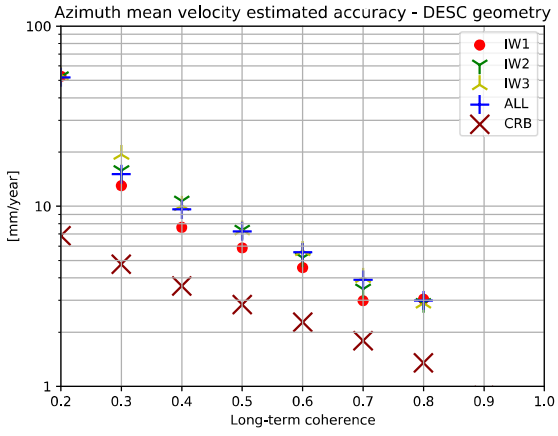

(f) Descending. Standard deviation of mean azimuth velocity

Fig. 3: The upper maps show the mean azimuth ground velocity evaluated at the burst overlaps for ascending (a) and descending (b). The maps at the middle part display the interpolated mean azimuth ground velocity for ascending (left) and descending (right). The 2013 surface rupture line, depicted with a solid black line, has been computed by Ken Hudnut from Caltech employing Landsat pixel offsets. The plots at the bottom show the standard deviation of the retrieved mean azimuth velocity computed over all overlaping areas of each subswath for different long-term coherences, the Cramér Rao Bound (CRB) values are shown for reference.